X-690-75-42
PREPRINT

NASA TM X- 70833

THE COMPLEX MAGNETIC FIELD OF JUPITER

M. H. ACUNA
N. F. NESS

FEBRUARY 1975

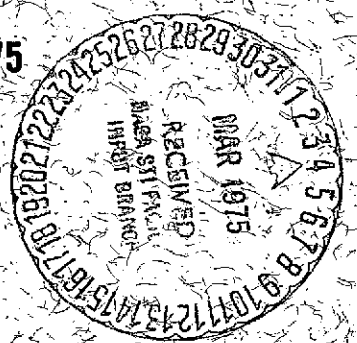

GSFC
GODDARD SPACE FLIGHT CENTER
GREENBELT, MARYLAND

For information concerning availability
of this document contact:

Technical Information Division, Code 250
Goddard Space Flight Center
Greenbelt, Maryland 20771

(Telephone 301-982-4488)

THE COMPLEX MAGNETIC FIELD OF JUPITER

by

Mario H. Acuna
Norman F. Ness

Submitted to Science
14 February 1975

ABSTRACT

The main magnetic field of Jupiter has been measured by the GSFC Fluxgate Magnetometer on Pioneer 11 and analysis reveals it to be considerably more complex than expected. In a spherical harmonic representation, the dipole term (with opposite polarity to Earth's), has a magnitude of 4.02 Gauss-R_j^3, at a tilt angle of 9.0° and a system III longitude of 221°. However, the quadrupole and octupole moments are proportionately very large, 50% and 90% of the dipole moment, and this leads to significant and complex deviation of the planetary magnetic field at distances $<4\ R_j$ from a simple dipole topology. The north polar field strength is 22 Gauss and in the northern hemisphere the "footprint" of the Io associated flux tube is localized to system III longitudes of 75°-215°. Associated L shell splitting in the radiation belts, warping of the equatorial planes, and enhanced absorption effects due to the satellites Amalthea and Io are expected as a result of the field complexity.

INTRODUCTION

Results from a preliminary analysis of the data for the NASA/GSFC magnetic field experiment on Pioneer 11 are summarized in this report. The high field triaxial fluxgate magnetometer (1) was provided by NASA/GSFC to extend the field range coverage up to 17 gauss, values believed to be representative of high latitude, low altitude field intensities from radio astronomy observations (2). The data have been analyzed in terms of a traditional Schmitt normalized spherical harmonic expansion fitted to the observations in a least squares sense. We show that the measurements can be interpreted in such a way as to add considerably to our knowledge of the main magnetic field of the planet. Our results have significant implications regarding theories of trapped radiation and radio emissions by Jupiter, absorption effects by the natural satellites and on general theories of planetary dynamos.

Previous Studies

The first in-situ studies of the magnetosphere of Jupiter were conducted in late 1973 by the Pioneer 10 spacecraft. An analysis of the Helium Vector Magnetometer data (3) indicated that the planetary field was well represented by an offset tilted dipole at distances from 2.8 to 10 R_j. Nevertheless, the moment (4.0 gauss-R_j^3) and tilt (10.6° at λ_{III}=222°) of this model yielded a field configuration and intensity which were inconsistent with a number of independently and previously derived estimates obtained from ground based observations of radio emissions (2). In contrast to the limited latitude and longitude coverage provided by Pioneer 10, the Pioneer 11 trajectory, which passed within 0.6 R_j of the planetary surface, covered 660° in longitude, from λ_{III}= 30° to λ_{III}=330°, and 80° in latitude, from -30° to +50° during the period of closest approach on December 3, 1974 from 0000 to 1100 GMT.

The measurements obtained over such a wide range of latitude and longitude provide a more complete sampling of the planetary magnetic field, which can then be analyzed with increased confidence to predict field values at other positions not covered by the spacecraft trajectory. The results of a preliminary analysis of the quick-look real time data obtained during Pioneer 11 Jupiter encounter by the GSFC-FGM instrument (4) indicated that within 3 R_j, the planetary field was much too complex to be represented by a simple offset tilted dipole and that higher harmonic multipoles were required. In this paper, we report the results obtained from an analysis of the preliminary experimenter's data tape covering the time interval 0120 to 0926 GMT (S/C time).

Instrumentation

The instrument consists of a single range triaxial fluxgate magnetometer sensor and associated electronics capable of measuring fields up to 10 Gauss along each orthogonal axis. Instantaneous vector measurements of the three components of the field, using a ten-bit precision A-D converter, yields a quantization step size of $\pm$600 gamma for fields less than 2 Gauss. These are made once every three revolutions of the spacecraft (36 seconds), in synchronization with a reference axis crossing through the ecliptic. The digitized data are sent directly to ground without further processing on board the spacecraft. The complete instrument weighs 272 grams and uses 300 milliwatts of power from the GSFC-Cosmic Ray Telescope Experiment. A more complete description has been given in (1).

The raw magnetic field data are translated to a Jupiter centered spherical coordinate system and combined with spacecraft trajectory positional information to yield a triad measurement set. A total of 683 vector measurements

were obtained during the close encounter period, corresponding to radial distances in the range $1.7\ R_j < R < 6\ R_j$. Due to the low spacecraft bit rate during occultation when the S/C was placed into a memory storage mode, no measurements were obtained in this period by this experiment.

Observations and Analyses

The predicted magnetic field components for the D_2 model of Smith et al. (3), and the GSFC-FGM observations have been plotted in a Jupiter centered spherical coordinate system as a function of radial distance as shown in Figure 1(a). For radial distances greater than $4\ R_j$ there is reasonable agreement with the predicted values, both in magnitude and polarity, although the quantization step size of the FGM instrument precludes a closer comparison when the measured field is less than 1000γ. The largest deviation is observed for $R > 4\ R_j$ in the radial component of the field. For distances less than $4\ R_j$ the observed field increases rapidly, much faster than the inverse cube law for a dipole model such as D_2. This implies that the contributions from higher order multipoles are significant and must be included in the analysis to obtain an adequate representation of the main planetary field.

The magnetic field $\vec{B}$ in a region containing no sources ($\nabla \times \vec{B} = 0$) can be expressed as the gradient of a scalar potential V which represents the contribution of sources internal and external to the region of interest. Thus we have

$$\vec{B} = -\nabla V = -\nabla(V^e + V^i) \qquad (1)$$

and it is customary to express the potential in terms of spherical harmonics as

$$V = V^e + V^i = a \sum_{n=1}^{\infty} \left\{ \left(\frac{r}{a}\right)^n T_n{}^e + \left(\frac{a}{r}\right)^{n+1} T_n{}^i \right\} \qquad (2)$$

where in our case r denotes the distance from Jupiter's center, a is Jupiter's radius (71372 km) and the $T_n^{e,i}$ are given by

$$T_n^i = \sum_{m=o}^{n} P_n^m (\cos\theta)[g_n^m \cos m\phi + g_n^m \sin m\phi]$$

$$T_n^e = \sum_{m=o}^{n} P_n^m (\cos\theta)[G_n^m \cos m\phi + H_n^m \sin m\phi] \qquad (3)$$

The angles ϕ and θ denote zenographic east longitude and co-latitude respectively, $P_n^m(\theta)$ are the associated Legendre functions with Schmitt normalization and g_n^m , h_n^m, G_n^m and H_n^m are the Schmitt coefficients.

From a well known theorem of potential theory, a unique representation of the magnetic field in the source free region is derivable from vector measurements over a simple surface which completely encloses the internal sources. In the case at hand, we do not have such a "complete" set of observational data and thus it is impossible to find a unique solution. Said another way, the data do not form an orthogonal set which span the same space as the harmonic representation. In practice, this means that cross coupling exists between the various harmonic coefficients g_n^m, h_n^m, G_n^m and H_n^m in that as the order of the representation increases from n=1, the values of the coefficients so derived vary, dependent upon the highest order employed. We shall see these effects in the hierarchy of solutions presented later.

With respect to the validity of the source free region approximation, we have estimated the diamagnetic effects of the trapped charged particles (5) and the possible ring current effects due to their drift in the region $R < 10\ R_j$. We have also considered the fields due to the highly distorted distant magnetosphere or magnetodisc (3) which occurs at

distances $>25\ R_j$. The combined effects appear to be significantly less than the quantization step size, $\pm 600\gamma$. Thus a representation of a scalar potential is justified and all external fields have been assumed negligible in our data set (i.e. $G_n^m = H_n^m = 0$ for $n \geq 1$, $m \geq 0$).

The observations obtained between 1.7 and 6.0 R_j were fitted in a least squares sense to first, second and third degree spherical harmonic expansions of the form [2], (n=1,2,3), that is, terms corresponding to a centered dipole, quadrupole and octupole moments of internal origin only. Thus, given a set of measurements we compute a set of coefficients $\{g_n^m, h_n^m\}$ such that the sum over the N measurements of the vector residuals squared

$$\sum_{k=1}^{N} |\vec{\epsilon}_k|^2 = \sum_{k=1}^{N} \{ |\vec{B}_{model} - \vec{B}_{obs}|^2 \} \qquad [4]$$

is minimized. We find that the inclusion of quadrupole and octupole terms (n=2,3) leads to a significant reduction in the RMS of the residuals.

From the quadrupole expansion (n=2), an offset tilted dipole representation can be obtained using 6 of the 8 dipole plus quadrupole coefficients to model the field. In Table I, we show the results obtained for the dipole terms in different representations as well as the vector RMS of the residuals for each model. As previously noted, the dipole term is observed to vary, depending upon the highest order n of the representation used.

The dipole, OTD and quadrupole models yield vector RMS deviations which are considerably larger than the quantization step size of the instrument. Also, the dipole axis tilt is smaller than that inferred from radio astronomy observations although the longitude is in reasonable agreement with prior work (2). The octupole model on the other hand provides a much better agreement with the observations with a significantly reduced residual RMS. The dipole term in the octupole expansion also agrees much better with Pioneer 10 results derived from energetic particle measurements (5) and magnetic field observations (3). These facts are a clear indication that the main magnetic field of Jupiter is extremely complex and cannot be represented by any simple dipole models, especially for distances less than 4 R_j.

To illustrate the goodness-of-fit obtained with the octupole model, which we shall denote as O_3, a plot similar to the one shown in Figure 1a for the D_2 model of Smith et al. is shown in Figure 1b. The overall agreement with the observations is excellent in all three components of the field. There are suggestions however, that the inclusion of higher order terms of internal origin and external terms to at least first order, could further improve the fit to the observations and provide additional insight into the mechanisms responsible for the complexity of the observed field.

Interpretation

The magnitudes of the quadrupole and octupole moments calculated from the O_3 model are 49% and 89% of the dipole moment respectively. These large values lead to a very complex field topology which extends to significant distances from the planet. Figure 2 shows a plot of isointensity contours obtained from the model at the surface of the planet and at 2 R_j (a 1/15.4 flattening has been assumed for the surface plot). It is clearly evident that even at 2 R_j the magnetic equator, as defined by the minimum field

intensity, is highly distorted and bears little resemblance to that expected from any simple dipole model. Thus, in any attempts to reconcile the observed decimetric radiation from Jupiter with models of the radiation belts (6), a study which uses a specific field model, the real deviations from a dipole will be incorrectly treated by any interpretation which admits only a dipole in the modeling.

In general, the maps in Figure 2 show considerable hemispherical and azimuthal asymmetries. On the surface of the planet, the maximum field strength at the poles is highly asymmetrical, 22.8 and 15.8 Gauss respectively in the north and south polar regions, and much higher than that inferred from the D_2 dipole model. The map also shows that subsidiary maxima exist. These departures from symmetry lead to a very complex distortion of the motion of trapped particles forming the radiation belts (7). These observed strong azimuthal asymmetries are no doubt in part responsible for the periodic escape of relativistic electrons, as discussed in (8). The magnitude of the higher order moments is such that considerable L shell splitting is expected to occur even at large distances from the planet (7). We have calculated the corresponding L values derived from the O_3 model along the spacecraft trajectory for the particular case of 90° pitch angle particles, as shown in Figure 3. We have also shown the corresponding values for the D_2 model and a centered dipole model with 9.5° tilt at 233° longitude (5), as well as the range of L values covered by Io and Amalthea, based on O_3. Figure 4 provides more detailed information about Io and Amalthea L shell parameters. In particular, it can be observed that a broader range of L values than that predicted from dipole models is covered and the curves are asymmetrical

with respect to the zenographic phase of the subsatellite points.

The range and predicted crossing times of the L shells affected by these satellites are given in Table 2. The range of L swept out by the satellites Io and Amalthea is considerably larger than that expected for a dipole model and this predicts enhanced absorption effects of these satellites. The predicted L shell crossing times agree very well with the times derived from charged particle measurements (9) which show satellite sweeping effects. Thus, this provides a necessary independent test of the validity of the O_3 model. By comparison with the inferior predictions of the D_2 model, it is an indication of the improvement achieved with O_3.

The charged particle data obtained during the close encounter period (9) show 4 minima in count rate and 3 interior peaks. The two exterior minima can be explained in terms of Amalthea sweeping effects by the O_3 model. There exist three possible explanations for the one peak and remaining two minima which occur near closest approach. The most plausible is that the O_3 model does not include sufficiently high order terms (i.e. hexadecapole and beyond) and as such is limited in latitude and longitude resolution to determine fine L shell structure variations on this scale. The second explanation adds the existence of a significant longitudinal variation of the loss cone on an L shell and across L shells. Finally, although we consider it remote, the possibility exists that the two minima are due to charged particle sweeping effects by an unknown satellite or ring of particles not yet visually observed.

In Figure 4 is shown a set of parameters useful in studying the relationship of the trapped particle motions with the absorption effects

of the satellites Amalthea and Io. These data indicate in more detail than Figure 3 permitted the rather large extent of the L region affected by the satellites and the asymmetries which exist in the parameters due to the complex planetary field.

The magnetic equatorial distortion may also have significant implications regarding the efficiency with which satellites can sweep up trapped particles (10). We expect a large fraction of near equatorial pitch angle particles to interact with any satellite orbiting Jupiter in or near its equatorial plane. Further, if such is the case, the pitch angle distributions will not peak as markedly around 90° as predicted for a dipole model.

The concentration of field lines around the strong north pole, i.e., the localization in longitude and latitude, and the relationship to the field lines passing through Io may play an important role in explaining the modulation of the decametric emissions by this satellite. We show the "footprint" of the field line through the satellite Io in Figure 2 and is seen to pass through the north polar region where it is restricted to system III longitudes lying between 75° and 215°. In the southern hemisphere, the footprint passes near the south pole and covers a greater longitude range between 130° and 360° with a minor trace from 0° to 30°. These features indicate that particles mirroring on Io's L shell also mirror in the Zenovian auroral regions. With the larger fields in the north, then the primary source of decametric radio emissions is probably sporadic precipitation of particles into the northern hemisphere. If we assume that the observed frequencies correspond to electron gyrofrequencies near the surface of the planet,

we predict 25 to 64 MHz for the north polar region, and 22 to 33 MHz for the south polar region. This implies, of course, that the precipitating particles radiate their energies and interact with the ionosphere at higher altitudes since the maximum observed frequency of emission is 40 MHz (2).

In addition to testing the validity of the O_3 model by comparison of predicted and observed satellite sweeping effects, we have conducted another special test. This consists of assuming that the centered dipole representation derived by the Iowa group (5) is a better approximation to the dipole term than that of D_2 (3) or O_3. In order that our octupole representation approach that of a simple centered dipole at large distances, the charged particle data require that we constrain the ratios g_1^1/g_1^0 and h_1^1/g_1^0 so as to achieve a dipole tilt of 9.5° at a system III longitude of 233° (extrapolated by 3° from Pioneer 10 epoch).

The least squares fitting to our data with such a constraint yields a harmonic coefficient set nearly identical to the unconstrained O_3 model. The vector residual RMS is exactly the same as before, 0.015 Gauss and the dipole moment increases by 0.8% to 4.05 Gauss-R_j^3. The 15 individual harmonic coefficients change by very small amounts, ranging from 0.3% to 16% with an RMS value of 2.6%. Lastly, the isointensity contour maps show negligible deviations from those of O_3, as expected with such a coefficient set. Thus we conclude that O_3 represents a superior model of the main magnetic field of Jupiter for distances $\lesssim 6$ R_j and is probably valid at distances up to 12 R_j, the distance at which the effects of external fields of the magnetodisc will become important and must be included.

The large quadrupole and octupole moments have significant implications regarding the origin of the planetary magnetic field. It is widely accepted that the most plausible explanation of the Jupiter field is associated with an internal dynamo (11). Whether or not the mechanism is identical to Earth is of considerable importance. The large higher multipole harmonics suggest a much larger source region proportionately, than the Earth, i.e. a much larger "core" on Jupiter, proportionately.

Future Work

The results reported herein represent only our initial efforts of a more complete and detailed study of the Jovian magnetic field, its origin and effects on charged particles. In particular, we intend to improve on the O_3 model given here, by incorporating additional internal and external terms in the analysis, as well as global field characteristics deduced from charged particle measurements. From these studies an improved model should emerge which can be used with confidence to calculate L-shell structures, bounce and drifts periods, trapping boundaries and other relevant parameters to a more complete description of the Jovian magnetosphere.

Equally significant, the study of the model in the context of radio astronomy observations should provide us with an increased understanding of the mechanisms responsible for the emissions, and their modulation by Io as in the case of the decametric bursts. And lastly, a valid representation of the main field and its possible time variations, by comparison with similar analyses of Pioneer 10 data, should provide insight on any temporal variation of the magnetic field and the properties of the planetary interior. The differences between system III and system II may be due to a secular variation as observed in the Earth's field.

M. H. Acuna
N. F. Ness
Laboratory for Extraterrestrial Physics
NASA-Goddard Space Flight Center
Greenbelt, Maryland 20771

February 14, 1975

References

1. M. H. Acuna, N. F. Ness, Space Sci. Instrumentation, (1974), in press.
2. T. D. Carr, S. Gulkis, Ann. Rev. Astron. Astrop., 7, 577, (1969); J. W. Warwick, Space Sci. Revs., 6, 841, (1967); P. M. McCulloch, M. M. Komesaroff, Icarus, 19, 83, (1969) and references therein.
3. E. J. Smith, NASA-JPL Technical Report 616-48, (1973).
4. M. H. Acuna, N. F. Ness, Nature, 253, 327, (1975).
5. J. A. Van Allen, D. N. Baker, B. A. Randall, D. D. Sentman, JGR, 79, 3559, (1974).
6. G. L. Berge, Ap. J., 191, 775, (1974) and references therein.
7. J. G. Roederer, Revs. Geo. Sp. Physics, 10, 599, (1972).
8. T. W. Hill, J. F. Carbary and A. J. Dessler, Geophys. Res. Lett., 1, 333, (1974).
9. R. W. Fillius, A. Mogro-Campero, C. McIlwain, Science, this issue, (1975); J. Trainor, et al., Science, this issue (1975).
10. G. D. Mead, W. N. Hess, JGR, 78, 2793, (1973).
11. D. Gubbins, Revs. Geo. Sp. Physics, 12, 137, (1974).

12. We thank C. F. Hall, J. Lepetich and D. Sinott of the Pioneer Project Office at NASA Ames for their support during integration of this experiment. We especially thank Professor J. G. Roederer of the University of Denver for making certain of his computer programs relating to trapped particle motion available to us and G. Burgess, F. W. Ottens and R. F. Thompson of NASA/GSFC for their outstanding support in the prompt analysis of these data. We appreciate opportunities to discuss these results with J. K. Alexander,

S. Gulkis, J. Warwick and colleagues on Pioneer 11. Finally, the support provided by Mr. D. Stillwell of NASA/GSFC and the Space and Tactical Systems Corporation, Bedford, Mass. during the development of the instrument is deeply appreciated.

TABLE I

	Highest Term in the Expansion			
Dipole Moment (Gauss-R_j^3)	Dipole	OTD (n=2)	Quadrupole	Octupole
g_1^0	4.34	4.36	4.36	3.97
g_1^1	-0.179	-0.296	-0.295	-0.411
h_1^1	0.348	0.350	0.348	0.473
Moment	4.35	4.38	4.38	4.02
Tilt from Z axis	5.3°	$6.0^\circ \pm 1^\circ$	$6.0 \pm 1^\circ$	$9.0^\circ \pm 1^\circ$
Longitude (λ_{III})	$207^\circ \pm 10^\circ$	$220^\circ \pm 10^\circ$	$220^\circ \pm 10^\circ$	$221^\circ \pm 10^\circ$
Offset (R_j)				
X_o	NA	-0.075	NA	NA
Y_o	NA	0.033	NA	NA
Z_o	NA	-0.03	NA	NA
Vector RMS (Gauss) Residual	0.042	0.026	0.025	0.015

TABLE 2

Satellite =	Amalthea	Io	Europa
L Range	2.21-2.65	5.65-6.22	9.20-9.83
Predicted O_3 Crossing Times			
Inbound	0453-0459	0332-0346	0216-0231
Outbound	0602-0614	0658-0702	0722-0724

List of Figures

1. Comparison plots of spherical coordinate components of the GSFC-FGM magnetic field measured on Pioneer 11 with the simple offset tilted dipole model, D_2, (1a, left panel) and the GSFC octupole model, O_3 (1b, right panel).
2. Isointensity contour maps of the Zenovian magnetic field at the "surface" (upper panel) and at the assumed centroid of the decimetric radio emission region, $R = 2\ R_j$ (lower panel). The significant distortion of the minimum B surface from a plane is evident, as is the localization of the northern footprint of the Io associated flux tube. The trace of the Pioneer 11 trajectory near perijove is indicated in the upper panel.
3. Comparison of three different magnetic field models in terms of the derived equivalent L shell parameter. Note the convoluted behavior of the GSFC O_3 model result near closest approach when compared to either Pioneer 10 models, D_2 or "Iowa", both extrapolated to the epoch of Pioneer 11.
4. Illustration of the effect of the complex main magnetic field of Jupiter on the L shells affected by absorption effects of the satellites Amalthea and Io. The equatorial points of the field lines threading the satellites, field magnitude and distance and presented in the top two panels, and the actual L value at the satellite in the lower panels.

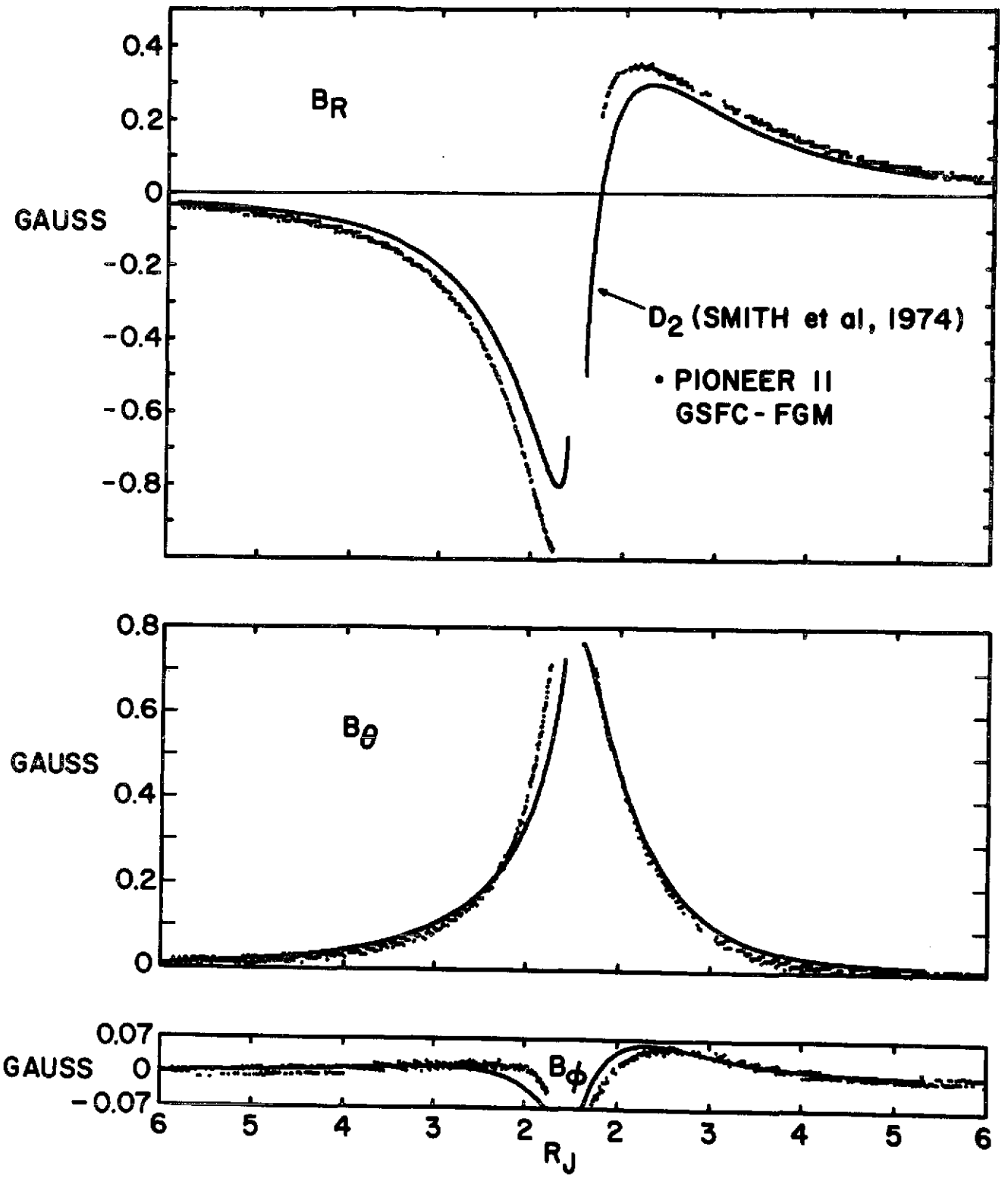
0.4
0.2
0
-0.2
-0.4
-0.6
-0.8
GAUSS
B_R
D_2 (SMITH et al, 1974)
• PIONEER 11
GSFC - FGM
0.8
0.6
0.4
0.2
0
GAUSS
B_θ
0.07
0
-0.07
GAUSS
B_ϕ
6
5
4
3
2
2
3
4
5
6
R_J

FIGURE 1a

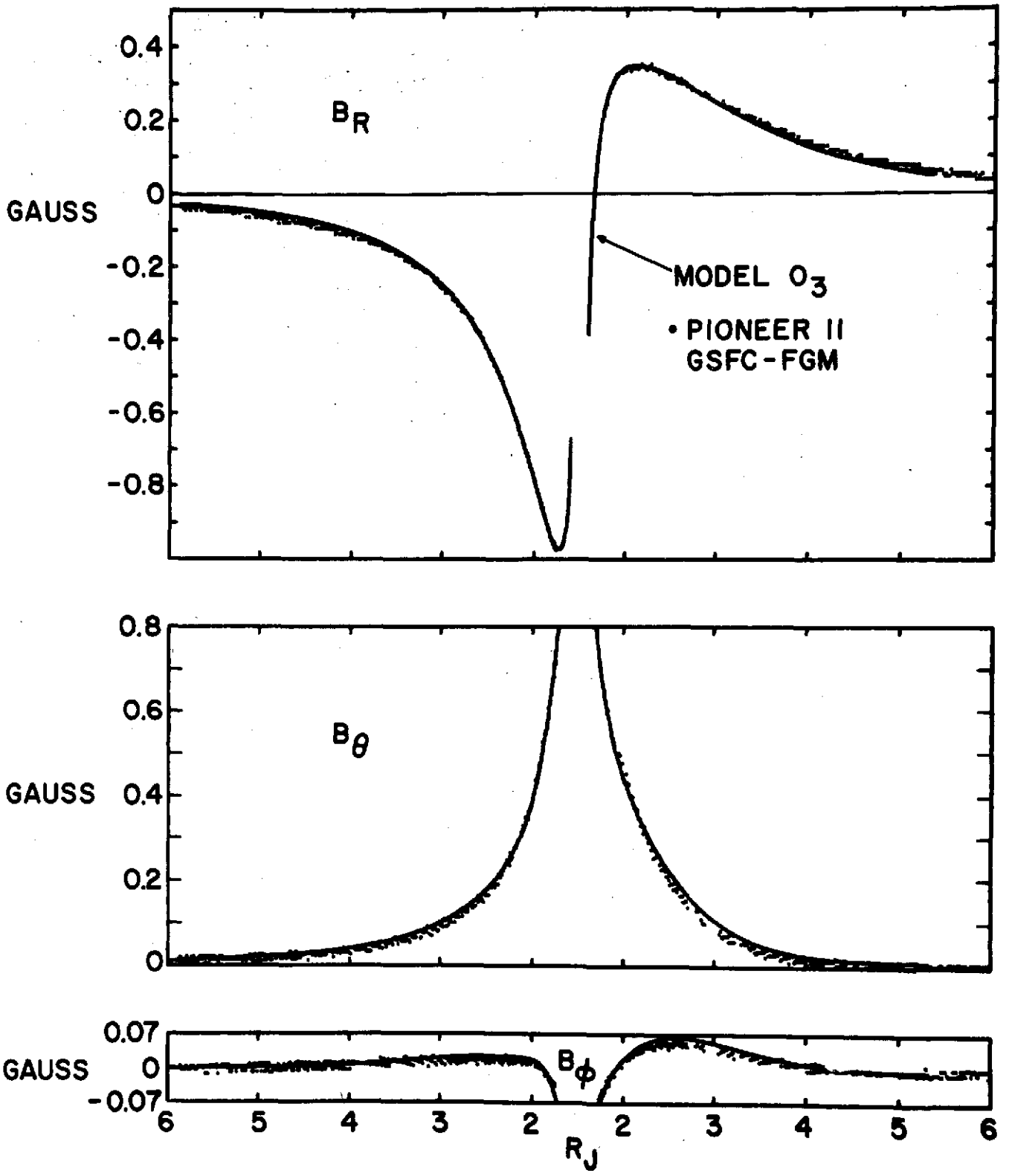
0.4
0.2
0
-0.2
-0.4
-0.6
-0.8
GAUSS
B_R
MODEL O_3
• PIONEER 11
GSFC-FGM
0.8
0.6
0.4
0.2
0
GAUSS
B_θ
0.07
0
-0.07
GAUSS
B_ϕ
6 5 4 3 2 2 3 4 5 6
R_J

FIGURE 1b

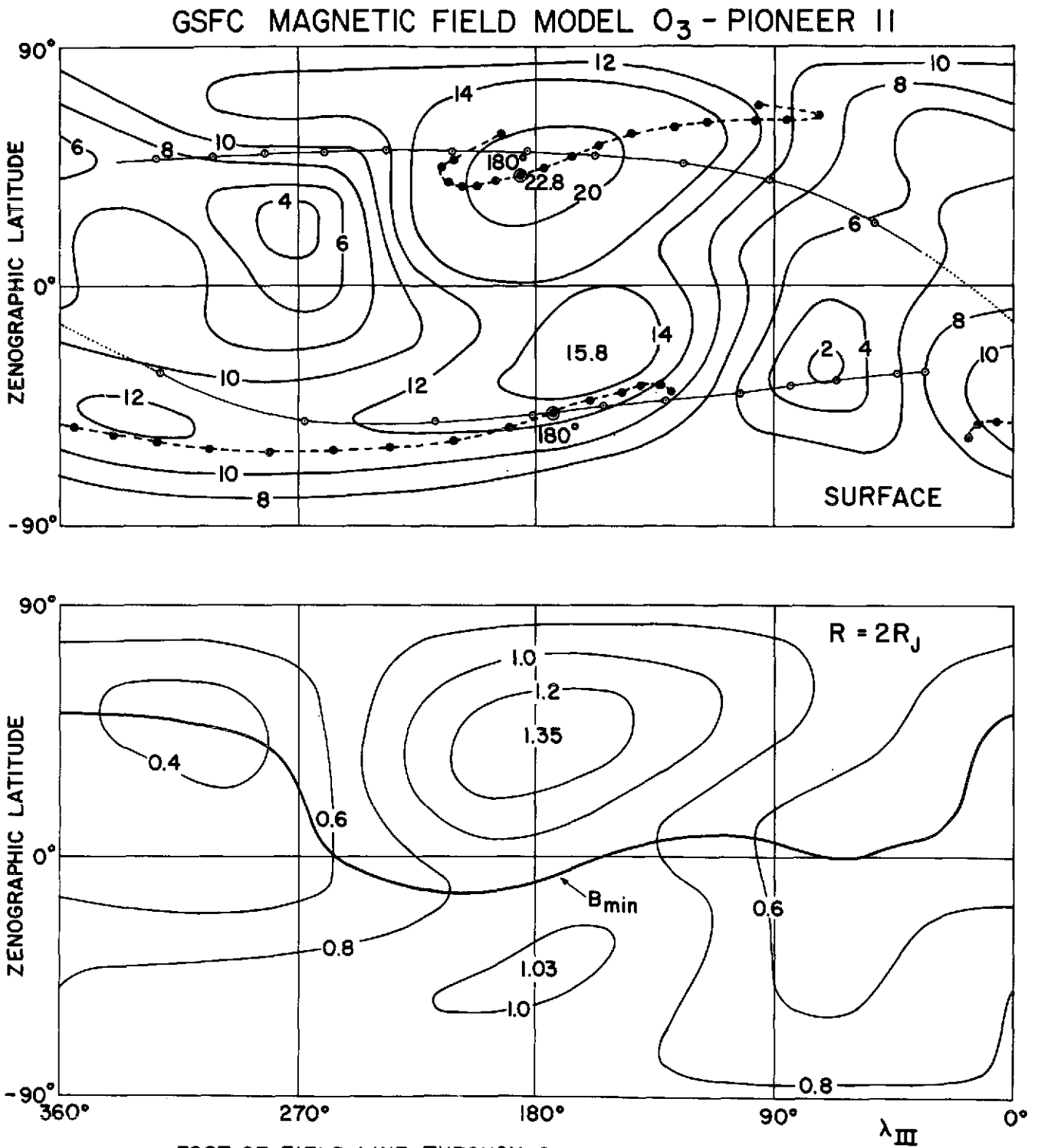
GSFC MAGNETIC FIELD MODEL O_3 - PIONEER II
90°
0°
-90°
ZENOGRAPHIC LATITUDE
SURFACE
R = 2R$_J$
B_{min}
360°
270°
180°
90°
0°
λ_{III}
FOOT OF FIELD LINE THROUGH Io
SUB-PIONEER II TRACE
MAGNETIC EQUATOR

FIGURE 2

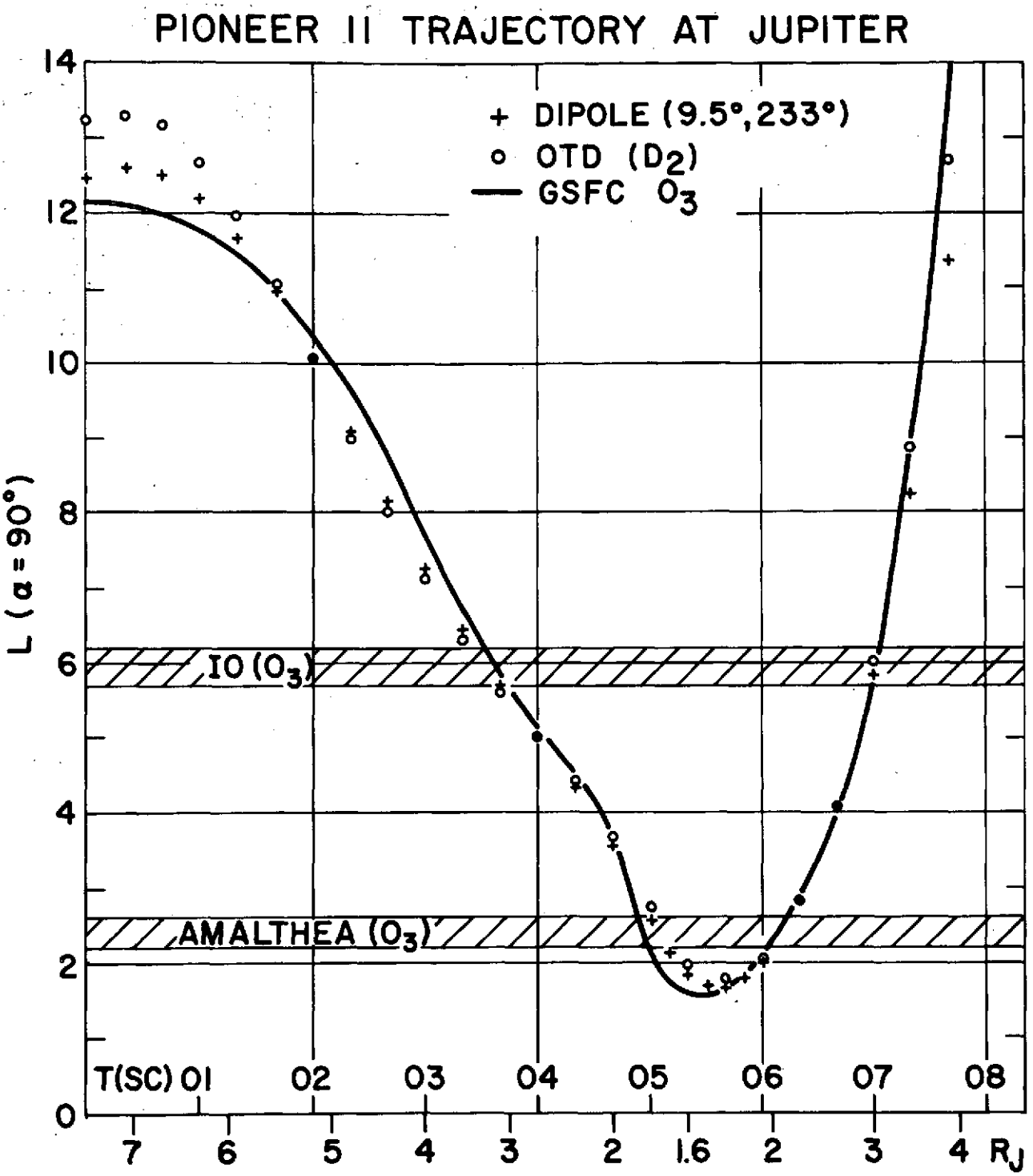
PIONEER 11 TRAJECTORY AT JUPITER
+ DIPOLE (9.5°,233°)
o OTD (D_2)
— GSFC O_3
L (α = 90°)
IO (O_3)
AMALTHEA (O_3)
T(SC) 01 02 03 04 05 06 07 08
7 6 5 4 3 2 1.6 2 3 4 R_J
0 2 4 6 8 10 12 14

FIGURE 3

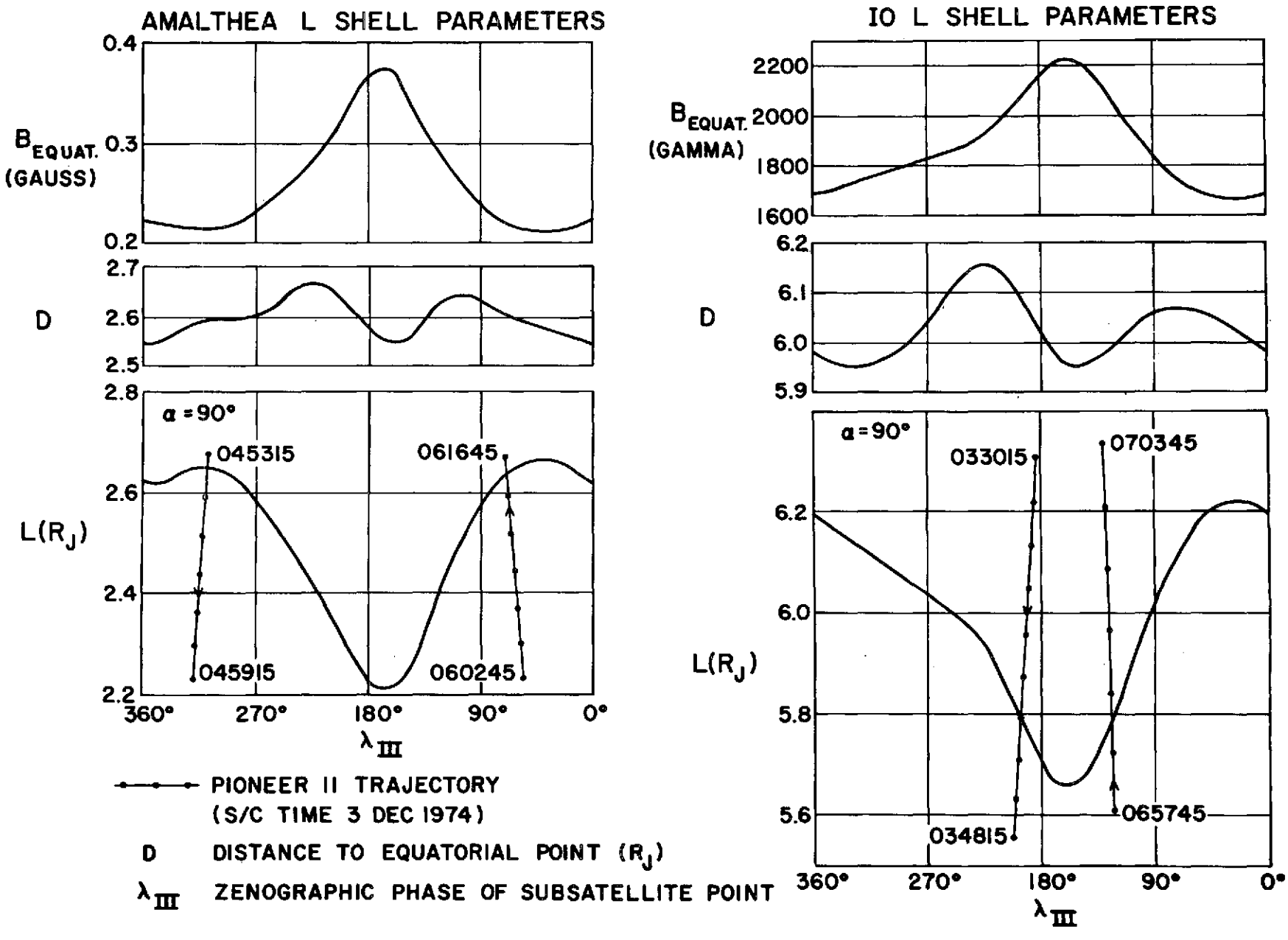
AMALTHEA L SHELL PARAMETERS
$B_{EQUAT.}$ (GAUSS)
0.4
0.3
0.2
D
2.7
2.6
2.5
L(R_J)
2.8
2.6
2.4
2.2
α = 90°
045315
061645
045915
060245
360°
270°
180°
90°
0°
λ_{III}
PIONEER 11 TRAJECTORY
(S/C TIME 3 DEC 1974)
D DISTANCE TO EQUATORIAL POINT (R_J)
λ_{III} ZENOGRAPHIC PHASE OF SUBSATELLITE POINT
IO L SHELL PARAMETERS
$B_{EQUAT.}$ (GAMMA)
2200
2000
1800
1600
D
6.2
6.1
6.0
5.9
L(R_J)
α = 90°
033015
070345
034815
065745
6.2
6.0
5.8
5.6
360°
270°
180°
90°
0°
λ_{III}

FIGURE 4